Additive Manufacturing 64 (2023) 103437

Contents lists available at ScienceDirect

Additive Manufacturing

journal homepage: www.elsevier.com/locate/addma

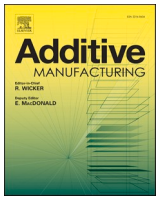

Closed-loop direct ink extruder system with multi-part materials mixing

Markellos Ntagios [a], Habib Nassar [a], Ravinder Dahiya [b,*]

[a] James Watt School of Engineering, University of Glasgow, G12 8QQ, Glasgow, UK
[b] Bendable Electronics and Sustainable Technologies (BEST) Group, Electrical and Computer Engineering Department, Northeastern University, Boston, MA 02115, USA

ARTICLE INFO

Keywords:
3D printing
Additive manufacturing
Embedded systems
Multimaterial printing
Smart structures

ABSTRACT

The field of additive manufacturing has expanded from single material-based 3D printing to multimaterial printed complex smart structures with intrinsic sensing capability. However, current multimaterial 3D printers allow printing of one material at a time, with limited ability of mixing multiple materials. Herein, we present the new 3D printer which eliminates the above shortcoming by merging the Fused Filament Fabrication and Direct Ink Write in one compact system. The developed printer expands the range of materials that can be printed and allows mixing and printing of multi-part materials with cost effective parts and increases the printing window of complex materials such as two-part rubbers. The experiments performed using various materials show the developed 3D printer having good control even at high printing speeds (up to 20 mm/s). The performance of the printer was evaluated extensively by varying different parameters such as nozzle diameter, pressure and printing speed. Finally, the capability of developed printer is demonstrated by autonomous printing of various 3D smart structures.

1. Introduction

Additive manufacturing (AM) is a fast growing field with rapidly evolving 3D printing technologies and their applications [1,2]. The easy availability of designs through open-source platforms has contributed to this growth as researchers and enthusiast can easily develop various types of complex and smart structures [3–5]. New printing materials too have been explored recently to incorporate functional elements in the printed smart structures for application in automation, biomedical instrumentation, aerospace, and robotics [6–11]. In this regard, the recent advances via multimaterial printing technology are noteworthy, as it has allowed expansion of 3D printing to develop advanced products such as artificial robotic/prosthetic hands with intrinsic touch sensing, various types of sensors [6,8,12–16], 3D printed antennas [17] and interconnects [18–20] etc. These advances provide attractive resource efficient route for fabricating sensorised objects, which do not experience typical wear and tear and hence offer robust solutions to putting sensors on the top of object's surface, as in the case of electronic skin for robots [21–24]. These smart objects are more robust as printed electrical interconnects could allow embedding of electronics [25–27].

In recent years, 3D printers have been heavily modified to expand their capabilities using variety of methods depending on the desired outcome. For example, researchers have developed manipulators and attached them, on 3D printers for pick and place functionality with optical cameras as feedback [28]. Likewise, extruder mechanisms have been developed for deposition of pastes to develop interesting solution for biomedical and electronic applications [29–33]. Some of those modifications are based on Direct Ink Writing (DIW) deposition methodology. DIW systems have focused heavily on optimizing the printing of materials with similar viscosities, narrowing the range of materials that can be used. Often Luer-lock needles are utilized as the tip of the extruder. Despite the advantage of easily changing the nozzle diameter, this approach increases the chance of clogging and altering the flow rate of the material over time and limiting the printability window [34–36]. In order to combat this drawback, high pressure is applied with an increasing risk of hazards. Further, many of the DIW extruders use direct drive systems which lead to uncontrollable deposition after start and stop commands, oozing and occasional inability to retract the material [37–39]. Importantly, most of these systems can only print one material at a time, they do occasionally allow mixing of multi-part materials, and thus cannot be used for advanced structures based on complex materials. Even the most recent systems suffer from the aforementioned problems [40].

The vast majority of DIW 3D printers are based on pneumatic actuation. Those systems require air pressure to work often delivered from a compressor or occasionally from a pre-pressurized cylinder [41]. These

* Corresponding author.
E-mail address: r.dahiya@northeastern.edu (R. Dahiya).

https://doi.org/10.1016/j.addma.2023.103437
Received 23 June 2022; Received in revised form 18 January 2023; Accepted 30 January 2023
Available online 1 February 2023

add to the cost and bulkiness of the systems making them unportable and noisy. Those systems often utilize the pressure to push on a syringe's piston mounted on the 3D printer's carriage to dispense the material in the syringe. The pressure is monitored and controlled from the valve that connects the pressured gas and the syringe. Other systems utilize pumps pushing the material stored in a reservoir [42,43]. These types of extruders lack feedback as the motor is controlled in similar ways as Fused Filament Fabrication (FFF) extruders. A minority of such system have implemented mixing of materials in some occasions [41,42,44]. The mechanisms that implements the mixing procedures do not utilize feedback therefore control of the flow is limited as those mechanisms which are often located close to the nozzle of the system [45].

Other printing techniques are the inkjet and aerosol jet printing [46–49]. These techniques utilize the piezoelectric effect or mix the air with the material to deposit on a substrate. These systems are often used to produce 2D structures and are difficult to integrate with other 3D printing techniques. The controlled mixing of materials together, while the printing process is ongoing, is very challenging. The utility of these deposition techniques is also limited by the viscosity of materials, limited variety of inks and the higher cost of inks. They also suffer from nozzle clogging and require frequent cleaning. Printing using these systems is also slower as compared to other printing methods.

These technological limitations, restrict the fabrication of smart objects and are currently obtained by other processes or at best by printing one material at a time. These increase the time of fabrication by adding multiple fabrication processes. In addition to being time consuming, the current approach limits the range of functionalities and applications. For example, multimaterial printing, with mixing of materials (e.g, soft multipart polymers mixed with magnetic particles or similar nanocomposites), could allow smart structures to have unique properties not possible with one type of material at a time. The desktop 3D printers with such a capability could considerably push the application domain for additive manufacturing. However, current FFF systems able of mixing materials are bulky, expensive and do suffer, in many cases, from deposition control difficulties. The new custom-made 3D printed DIW extruder system presented here (Fig. 1) removes this bottleneck.

Furthermore, a few of these systems have been developed to enable mixing of complex multi-part materials. Often, they use two syringes that are driven by separate actuators to push the materials. The syringes do not have any active mixing arrangement and normally there is a nozzle to allow materials to extrude. This type of arrangement may result in an non-uniform mixing of the material [50]. This issue can be addressed by introducing new arrangement for active mixing of the material. The active mixing is very much required for uniform printing of various types of materials [51].

The 3D printed DIW extruder system (Fig. 1) presented here utilizes a double extrusion mechanism and pressure sensor for feedback. The DIW extruder uses 2 stepper motors and off-the-shelf control electronics, simple design of supporting mechanical structure, resulting in an inexpensive system which is affordable even for hobbyists. The system is capable of mixing multipart material systems in different ratios and prints them to develop innovative smart structures. Materials such as Polydimethylsiloxane (PDMS) or Ecoflex can be printed with no need for manual mixing and thus providing better control of deposition and increases the printing window. The system shows no leaking issues compared to other systems while also being fairly compact, lightweight and portable. The developed printer offers significant advantages with respect to currently available DIW systems which require change of the flow rate of materials after a short period of printing [34,35] and also suffer from clogging of extrusion tip. Further, these systems have limitations on the size of the syringes that are compatible with the systems [37,38,40,52].

This paper is organized as follows: Section 2 describes the design of the developed system. The experimentation and results are presented in Section 3. In Section 4 we present the use cases showing the capability of

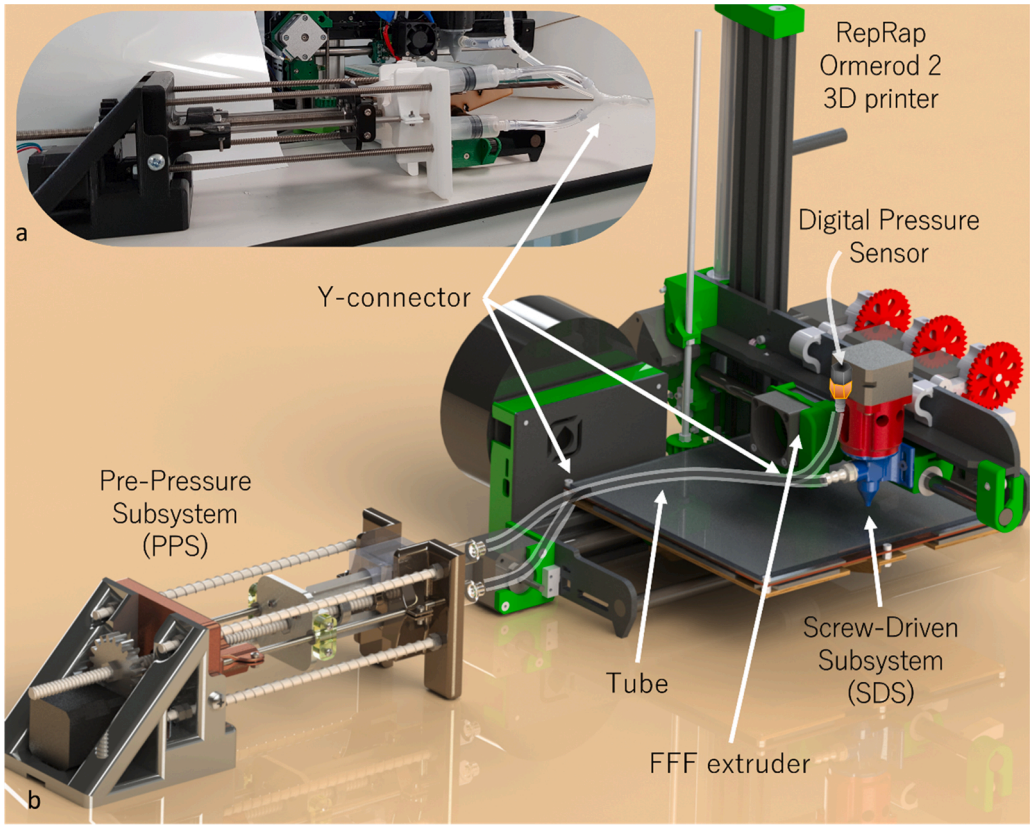

Fig. 1. a) Fully assembled customized 3D printer with in-house DIW system, b) CAD representation of the custom 3D printer.

the developed DIW printer. Finally, Section 5 summarizes the key outcomes of this work.

2. Materials and methods

The developed DIW system (Fig. 1) can be divided into two subsystems which are complementary to each other. The first is a Pre-Pressure-Subsystem (PPS) (Fig. 2) and the second is a Screw-Driven-Subsystem (SDS) (Fig. 3). All the parts were designed in a Computer-Aided-Design (CAD) program (SolidWorks) and most of these were fabricated using a Fused Deposition Modelling (FDM) 3D printer (S5, Ultimaker).

2.1. Pre-pressure-subsystem design

The PPS system, shown in Fig. 2, uses a stepper motor to convert the rotation motion to linear. Specifically, the PPS is designed to mount two syringes, one placed on the top and a second inserted from the bottom of the PPS (Fig. 2a, 2b). The syringes are attached with female Luer to Barb hose adapters and are connected together with flexible tubes (8 mm external diameter Flexible PVC, RS Components) and a Y-connector (Fig. 1). The common output from the syringe connector is connected to a tube and its ending splits again with another Y-connector. One end is connected to the pressure sensor (PX3AN2BS100PAAAX, Honeywell) and the second is connected to the inlet of the SDS system (Fig. 1).

The syringe barrels are placed on a large piece of Polylactic acid (PLA) support structure (Syringes Holder Fig. 2c) which incorporates the syringes holder at the front of the PPS system (Fig. 2c). The barrel parts of the syringes are secured and cannot move or rotate. The PPS core is an 8 mm threaded rod (leadscrew mechanism), as shown in Fig. 2. The threaded rod is attached to a 2:1 ratio 3D printed drive gear system. The driving gear is connected to a Nema 17 stepper motor, that drives the system. A leadscrew is located in the middle of the threaded rod and is attached to two pieces of PLA (namely enclosed structure) that encloses the leadscrew. The largest of the two pieces is designed to attach the two syringe plungers whereas the sides of the that part are attached to two linear bearings which restrict the entire structure from rotating but allow the system to move forwards and backwards along the threaded rod's length. The threaded rod is attached to the threaded rod base piece that has a narrow gap for the rod to barely go through. Two roll bearings are placed at the opposite sides of the narrow gap but are not able to go through. Two nuts then follow and are firmly attached next to the bearings. This arrangement allows the threaded rod to rotate freely, but the rod is restricted from moving backwards or forwards from its position (Fig. 2b). The three largest structures, namely the syringe base, threaded rod base and motor base, are attached to each other using four smaller threaded rods and nuts to allow for adjustments and better alignment of all the parts of PPS. This means that once the motor rotates, the plunger holder (Fig. 2c) is able to travel back and forward along the length of the threaded rod and in turn, move the plungers of the syringes. This pressurizes the material in the syringes and pushes or retracts the material.

2.2. Screw-driven-subsystem design

The material in the syringe travels from the PPS through the tube and ends in the inlet of the SDS. The SDS pushes the multi-material out of the outlet onto the bed of the printer. The SDS is a screw-based mechanical design (Fig. 3a). Fig. 3b depicts the fully assembled SDS design in CAD. The system's crucial component is a helical/screw structure, as seen in the cross-sectional view in Fig. 3c. The shaft of the screw passes through an oil ring that prevents printing material from leaking upwards and out of the system and allows the part to rotate with minimum friction. The shaft of the screw is then attached to the motor connector piece which itself is attached to the motor shaft. This arrangement transfers the rotation of the motor shaft to the helical/screw part in a 1:1 ratio. The oil ring is epoxied on the gear housing part of the SDS. The housing part is attached to the rotor and the nozzle part via M3 bolts and nuts. The nozzle piece of the system has gaps on one of its sides for M3 bolts which are attached to the 3D printer's x-carriage. The gaps allow the system to slide up and down to adjust the nozzle height on the printer.

The chamber that houses the screw is cylindrically shaped and is 12 mm in diameter and has a total length of 40 mm. In the last 12 mm of the chamber's length, the diameter decreases smoothly. This reduces the pressure drop from the screw to the outlet. This reduces the need for high pressure extrusion due to Poiseuille law as the length of the material that needs to be travelled from the source of the pressure (SDS helical screw) to the outlet is less than 3 mm. The screw's diameter has a 0.2 mm offset from the chamber's walls. The smaller the gap between the chamber's wall and the screw, the harder it will be for material to

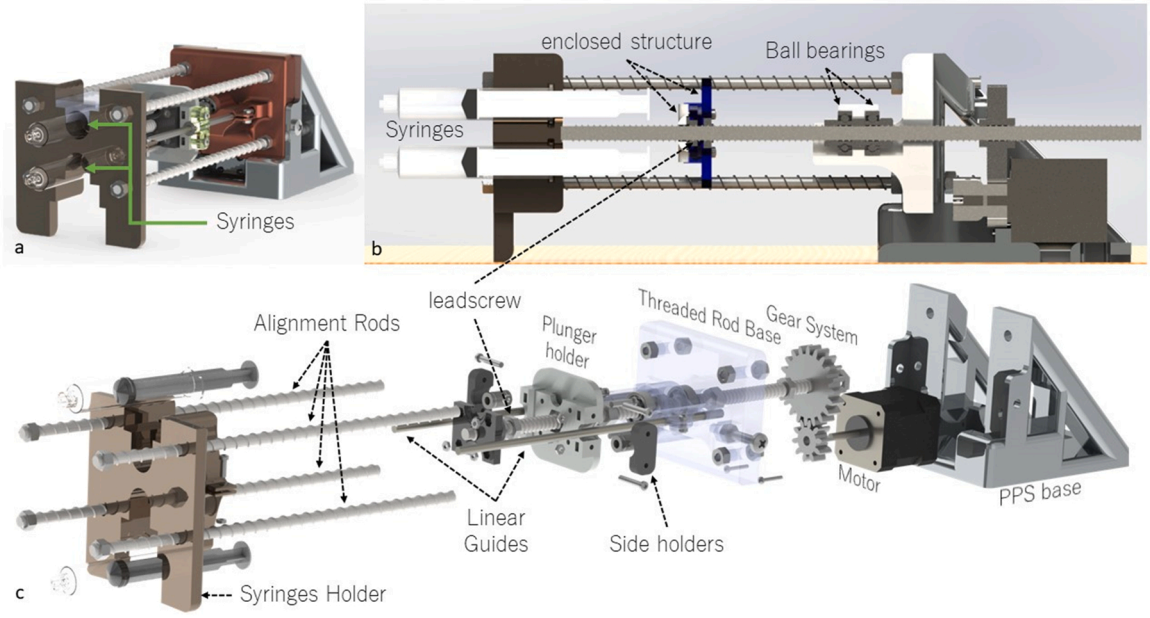

Fig. 2. a) CAD design of the assembled PPS system. b) Cross Section view of the PPS system. c) Exploded view of the PPS system.

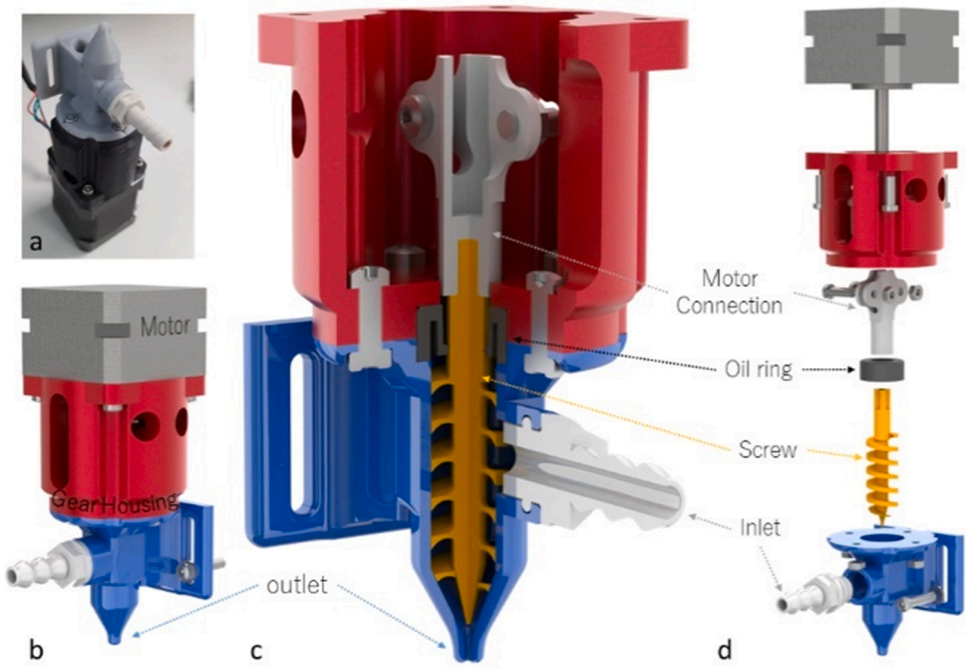

Fig. 3. a) Fully assembled SDS. b) Assembly CAD design. c) Cross-sectional view of the subsystem. d) Exploded view of the subsystem.

slip through the gap. The small gap also prevents the backflow up the side of the wall and helps build pressure to extrude material from the nozzle at the bottom of the screw. The screw has a pitch of 5 mm and 6 complete revolutions. Two nozzles were fabricated for the purpose of testing the system's performance under different outlet diameters. The first nozzle has a diameter of 1 mm and was obtained using a (FDM) 3D printer and the second is a 0.5 mm nozzle obtained using a Stereolithography (SLA) 3D printer.

The proposed SDS system offers substantial advantages over the Bowden-tube systems, which are typically used in DIW systems. The Bowden tube-based systems have drawbacks such as difficulty in controlling the amount of extruded material. Further, the need for pressure build up in these systems and the large distance between the syringe and the nozzle can prevent accurate translation of the motor's rotation to material extrusion [53]. These problems are addressed by SDS mechanism, which is also advantageous over other mechanisms for application of pressure such as pneumatic systems. Such systems also have difficulties related to integration with existing electronics in the FFF systems, require pressurized cylinders/compressors, and occasionally do not reproduce the same flow rates [40,54,55]. Further, pneumatic systems are often expensive and immobile. The system presented here demonstrates a portable alternative via utilizing a PPS with pressure feedback for pressure control and monitoring. This is achieved whilst reducing the cost and providing the ability for the system to be integrated with the existing electronics of FFF printers.

2.3. Electronics and integration

The PPS and SDS are controlled by two different electronics boards. Whilst PPS is controlled by a custom-made electronics board based on an Atmel microcontroller (Fig. S1), the SDS is controlled via the FFF printer's electronics. The extruder system was attached to an open-source 3D printer (Ormerod 2, RepRap, Fig. 1) which was modified for the purpose of this integration. The arrangement includes mechanical support and attachment parts of the SDS to the carriage of the printer. The SDS and the 3D printer are controlled by the Duet 3 Main Board 6HC (Duet3D). The stepper motor of the SDS is connected to the second extruder stepper driver. The Duet controls the SDS stepper motor in a similar way as it controls any other FDM feeder motors. In the firmware, a second extruder is enabled with cold extrusion, to bypass the detection of a heating element at the nozzle, and the step per mm is set to 80 steps per mm. Explanation of how this number is derived can be seen in the Supplementary Information.

For the PPS, a custom Printed Circuit Board (PCB) was designed, and an Atmel microcontroller was programmed to control the system. The stepper motor of the PPS is connected to PCB and is driven by a DRV8825 stepper motor driver (JYOPTO). The DRV8825′s digital input pins are connected to the microcontroller and the system was set up in a half-stepping mode. The pressure sensor, which is located near the inlet of the SDS, provides pressure feedback for the PPS and it is connected to the Atmel microcontroller. The pressure sensor outputs voltage varied between 0 and 5 V for a pressure range of 0–100 PSI. The voltage is measured by the Atmel microcontroller and translated to pressure value. The user can control the PPS either manually, where they control the speed and distance of the plunger, or set it to automatic mode where the microcontroller linearly displaces the plunger until the desired pressure is obtained. The Duet board and the Atmel were connected to each other via one Input Output (I/O) pin. The Duet 3 Mainboard 6HC has 9 I/Os that can be used to output 3.3 V logic signals and one of them was used here to output a signal to the microcontroller via the GCode. The Duet controls the pin's digital output, and the Atmel receives the information. The Duet board can set the pin to 'high' to indicate that the 2nd extruder is currently active and 'low' to indicate that it is inactive. That was done by modifying the GCode. The output signal generated in this way was then read by the microcontroller and the PPS system was driven as per user preferences. The PPS also utilizes an end-stop switch which, when pressed, allows the system to recognize that the material in the syringe is depleted. To this end, an LED is used as a visual indicator. A custom-made user interface (UI) made in Visual Studios was programmed in C# to visualize the pressure, control the PPS, and record the data and state of the system (Support Fig. S2).

3. Results

Two different material formulations, targeting different applications, were printed using two different nozzle diameters (0.5 mm and 1 mm).

The first material tested was a food condiment (mayonnaise, Hellman's Real) and the second is a two-part Silicone rubber (Polycraft GP-3481F RTV, Polygraft). The rheological properties of these materials are different from each other and hence they provide a good challenge to the system. The food condiment's viscosity was about 65,000 cp for low shear rates. It decreased with increasing shear rate and finally settled at 5000 cp at 2.5 s^{-1}. The base material of Silicone rubber showed an average viscosity of 39,000 cp before adding the catalyst (Fig. S3). To evaluate the system, we also varied the printing parameters such as pressure, printing speed and material flow.

The developed system was characterized for the line width deposited using each set of printing parameter that we altered. All data points from the tests are given in Table I of supplementary information. Two test structures were used for the evaluation of developed system. The first test structure design was a model containing 5 straight lines with length of 10 cm, width of 1 mm, and height of 0.5 mm. Both nozzles (1 mm and 0.5 mm) were used for this design. The second test structure is a CAD design containing 5 lines with 0.5 mm width, 10 cm length, and 0.25 mm height and it tested only with the 0.5 mm diameter nozzle. It is generally suggested to print using a layer height that is half the nozzle's diameter and this is the reason for difference between the two test designs. A few printing parameters were constant in all the characterization processes. These are: all walls were removed from all settings (bottom/top, sides), 100 % infill, heated bed was off and printing was carried out at ambient temperatures.

3.1. Printing pressure

Firstly, the materials were tested under pressure without printing to extract the suitable pressure range. Each material is mounted on the system individually, pressure is slowly increased to observes when and if the material would start oozing from the nozzle. The food condiment was not oozing from the nozzle for pressures up to 1 PSI. In contrast, the silicone-based material started oozing at pressures of 0.5 PSI. Following this, the constant pressure of 0.5, 1 and 1.5PSI were used for models mentioned above. The rest of the printer parameters were unaltered and they were: printing speed is set to 5 mm/s and material flow set at 100 %. In total, 18 prints were obtained to extract the information for all pressures and system arrangements (3 pressure settings, 2 materials, 3 print setups). The print setups are, the model with 1 mm width design lines with the 1 mm nozzle, the 1 mm width design with the 0.5 mm nozzle and the 0.5 mm design with the 0.5 mm nozzle. Each print was photographed, and each line was analyzed for its average width and all 5 lines were averaged out.

Fig. 4a shows the average printed line width with respect to pressure for each setting. The results show that line width of both materials (silicone and food condiment) increases linearly with increasing pressure. The increasing slope means the thickness of the lines are increasing linearly with pressure while the deviation represents the non-uniformity of thickness of the line over its length. The average rate of change and standard deviation for condiment were 0.8 mm/PSI and 0.123 mm respectively and were 0.6 mm/PSI and 0.18 mm for silicone material. The calculations were made by measuring 100 points for each printed line. Five printed lines were made for each condition resulting to 500 data points. These values were then averaged to produce the results. Fig. 4b shows the percentage ratio between actual printing length over the designed line length. In some cases, the prints did suffer from insufficient flow of the material, resulting in prints having droplet like formation instead of an actual line. Fig. 4b show that this is particularly observed at low pressure (0.5 PSI). As the pressure increased the droplet like formation got minimized for both materials. Similarly, for the line width, the percentage print varied with pressure and also with the material. The higher the pressure, the more is the likelihood of print lines to be continuous and uniform. Fig. S4 in supporting information presents all these printed structures.

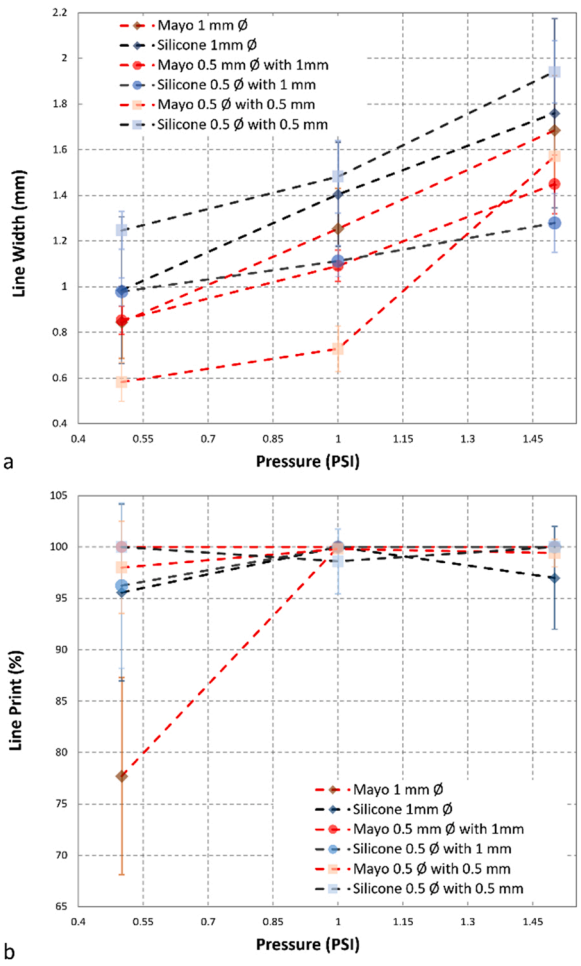

Fig. 4. Printing at different pressures. a) Average line width of 5 printed lines, b) Percentage ratio of printed lines length to designed length.

3.2. Printing speed

The second parameter used to characterize the system was printing speed. This was done to see how fast the printer can print reliably and the effect faster movements of printer on the line width. Each material was tested separately with the PPS providing a constant pressure of 1 PSI. The printing speeds tested were: 2, 5, 10 and 20 mm/s and a total of 24 prints were obtained. Fig. 5a presented the average linewidth for all 5 printed lines with respect to printed speed. Fig. 5b presents the percentage ratio between printed line length over designed length with respect to printed speed. These results show that the condiment material is less affected by printed speeds. On average all printed lines were continous, and the deviation is relatively low (average deviation for all print setting of the mayo is 0.088 mm). Materials with non-Newtonian rheological properties such as the condiment are affected by the SDS system as the rotation of the screw is affected by viscosity variations and the flow rate. The PPS acts as a tank for the SDS to control the deposition. The screw serves as an isolated piston and it deposits the material uniformly as long as there is enough material and pressure in the inlet. Therefore, speed does not have a significant affect on the prints. The rotation of the screw matches the printer's movement and therefore the amount of material deposited is the same.

In contrast to the above, the printing of silicone is affected by the speed. As the printer moves faster, the fast rotating screw cannot fully compensate for the amount of material that the PPS is contributing. Therefore, for same print, lesser material is extruded from the nozzle at higher speeds. On average, the line width decreased at a rate of

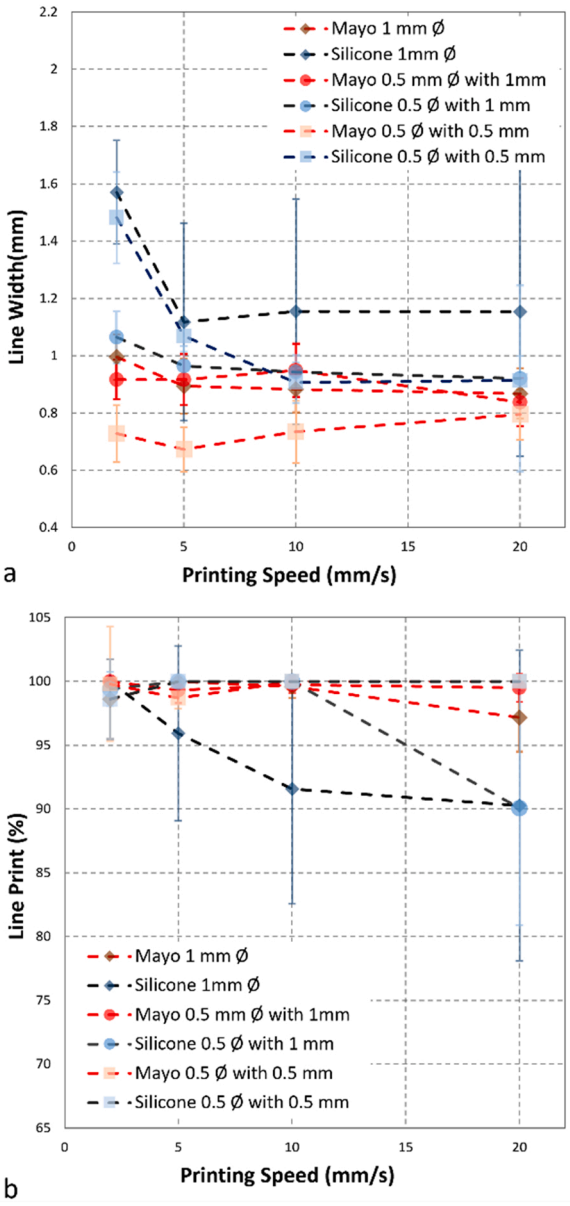

Fig. 5. a) Average line width with respect to speed b) percentage ratio of printed lines length to designed length with respect to printing speed.

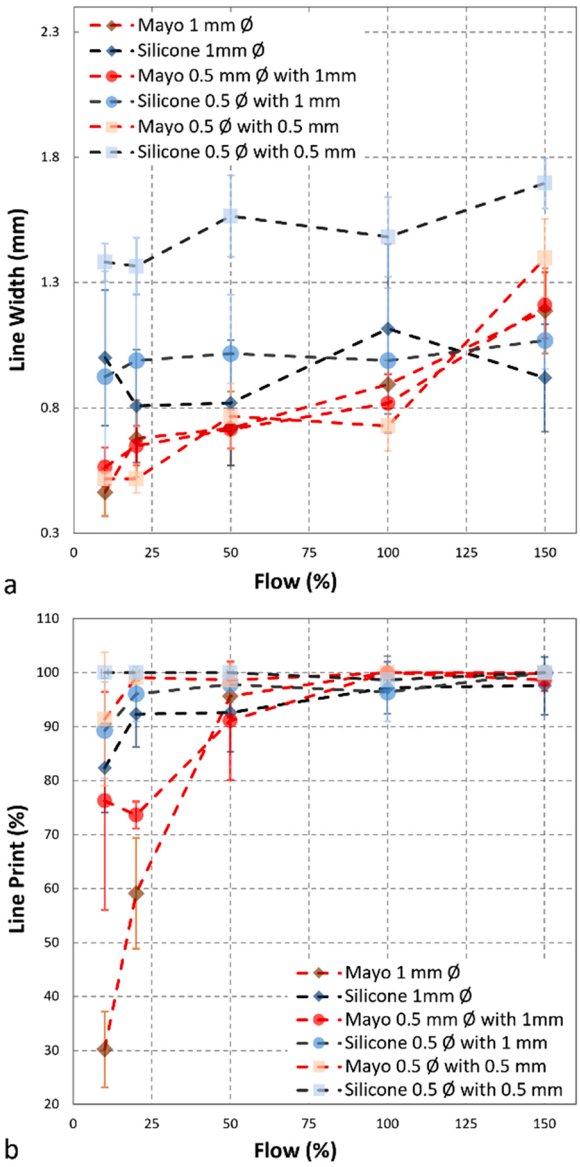

Fig. 6. a) Average line width with respect to percentage flow b) Percentage ratio of printed lines length to designed length with respect to percentage flow.

0.016 mm per mm/s, while the deviation from low speeds to high speeds increases rapidly. This further worsened when the print was evaluated for the percentage lengh printed over designed lengh. At low speeds, silicone has little droplet-like formation on the printed bed, but the effect is regular once the speed increses.

3.3. Printing with increasing flow

The last parameter tested was the percentage flow of the material. This setting changes the revolution percentage per mm of the screw. As discussed above, the rotation of the screw was set to 80 steps per mm. This means that the increase or decrease of flow is directly correlated with the number of steps the SDS systems rotate the screw in the same distance. This testing sets the effect of the ratio of revolutions of the SDS system per line. Five different flow rates were tested, namely, 10 %, 20 %, 50 %, 100 % and 150 % resulting in 30 different prints. Fig. 6 presents the data acquired from these tests. Fig. 6a shows the line width with respect to percentage flow. The percentage ratio of actual printed length (over the designed length) with respect to flow percentage is given in Fig. 6b.

This set of experimentation shows that SDS has greater influence on the mayo, while PPS has a greater influence on silicone. In fact, the line width of the silicone does not change significantly with increased flow. In contrast, line width of mayo changes with increased flow at a rate of 0.0047 mm per flow percentage. The relation between flow and line width is linear and the deviation for mayo is 0.11 mm. The screw rotates more times per line therefore more material is deposited on the printer bed. This is magnified even further when the percentage printed lines are compared to the expected lines. The flow of the material was too low to print continuous lines and droplets were observed in most of the print settings, especially for the prints with layer height of 0.5 mm. Once the material flow was high enough all prints were continuous.

In contrast to condiment material, silicone could flow easier in the chamber of the SDS, resulting in an added flow. Silicone does not provide any significant resistance and can flow from an inlet to an outlet even when there is a low amount of pressure. The screw does not provide a high amount of pressure difference between inlet and outlet for the silicone compared to the PPS that is the main contributor of the pressure difference for such materials. Even though the screw seems to have no

effect on the line width, it still provides some flow to the material. As can be seen in Fig. 6b, the faster the screw rotates, the less likely a droplet can form. That is caused by the screw's ability to push the material and at the same time allowing an even distribution of the pressure inside the SDS chamber. At 10 % flow silicone printed in more droplet-like forms. Once the flow setting was increased the droplet formation was minimized.

3.4. Increasing nozzle diameter

The effect the nozzle diameter has on the printing quality, could be derived from above experiments. For example, by comparing different nozzles (1 mm and 0.5 mm diameter) with the same CAD model (1 mm width lines at 0.5 mm layer height), it is easy to see the effect the nozzle diameter on the print lines. In fact, we observed that the nozzle diameter has a significant effect on the quality of the print. According to Poiseuille's law, the smaller diameter outlet should reduce the flow of material (under same pressure) resulting in deposition of lesser material on the bed. Both nozzles at low pressure show similar results but once the pressure increases, the width of the lines start to diverge with the wider nozzle diameter printing thicker lines compared to the narrower nozzle. The 1 mm nozzle showed an increase in line width of 0.841 and 0.775 mm/PSI for mayo and silicone, respectively. For the 0.5 mm diameter nozzle, the rates were 0.596 and 0.3 mm/PSI for mayo and silicone, respectively. Also, the narrower nozzle has lesser deviation in each pressure setting, thus increasing the uniformity in deposition.

The nozzles follow similar trend with respect to speed. The nozzle diameter shows little to no effect to line width when the food condiment is considered. For mayo, the SDS system significantly influences the material deposition, therefore, there is no significant change based on the nozzle diameter. Silicone has a small difference in the line width, with the narrowest nozzle depositing thinner lines. Likewise, when flow is considered, the nozzle diameter seems to play no role for the mayo as the difference in the print for both nozzles is insignificant. The nozzle diameter does not affect the line width, but can increase the reliability of the printing as it decreases the amount and length of discontinuous lines. The same is true for the silicone. The narrowest nozzle does not affect the printing lines width, but decreases the gaps between the prints.

4. Discussion

To illustrate the capability of developed system, a variety of test structures were fabricated as described below. All printing parameters are presented in Support Table II.

4.1. Two-part elastomer mixing and printing

A thin smiley face-like structure was printed using the developed 3D printer. For this, we used Ecoflex - an elastomer with two parts that are required to be mixed together for proper functioning. It is most commonly mixed in 1:1 ratio and wisely used as substrate in flexible electronics or to develop soft robotic structures. The CAD design resembles a face with two cheek bones, to evaluate the capability for z-axis printing of Ecoflex. The thickness of the smiley face was 0.6 mm and the bone cheeks reached a height of 2.8 mm with the face covering a circular area with diameter of 80 mm. The design was printed using 0.2 mm layer height at 100 % infill with a printing speed of 5 mm/s.

To fabricate the face design, the PPS was mounted with two identical syringes, each containing one part of the two-part elastomer at the same volumetric marker. This resulted in a 1:1 of part A and part B, mixed on the go inside the SDS chamber and printed on the surface of the 3D printer bed. For faster curing, the bed of the printer was heated at 40 °C. This also ensured that the subsequent layers printed on top have a solid structure for better resolution. The total time of the print is approximately 1 h. Once the print finished, the fabricated design was left for about 30 min at 40 °C on the print bed. Fig. 7a shows the printing of two-part elastomer and Fig. 7b shows the completed 3D printed the face-like structure. Support video 1 shows the entire printing process for realizing the smiley face.

4.2. Color mixing

To further validate the ratio printing and mixing procedure, a CAD file for disc-like structure was generated. Two different prints were carried out to demonstrate the mixing capabilities of the system. The PPS was mounted with two syringes, one containing a blue color paint and the second containing a white color paint. For the first print, both syringes have an inner diameter of 20 mm, therefore the ratio between the blue and white was 1:1. Figs. 8 and 9a shows the result of the printing process. The second print is the same disc design, but with different diameter syringes. The blue color paint was mounted on a syringe with diameter of 20 mm same as before, but the white paint was mounted on a syringe of 17 mm. The difference in surface area is 10:7 and the displacement of the syringes are identical. This results in a ratio of 10:7 for this print. Fig. 8b shows the result of this print, which clearly shows a different mixing ratio as the color of the printed structured has strong presence of blue color. The structures were printed with the PPS providing pressure of 0.5 PSI with a layer height of 0.5 mm and printing speed of 5 mm/s. Support Video 2 shows the real-time print of the two structures.

4.3. Food based materials

A major advantage of 3D printing is its versatility and possibility to alter the models without the need for fabricating different molds every time the design changes. This is further advanced with printing of

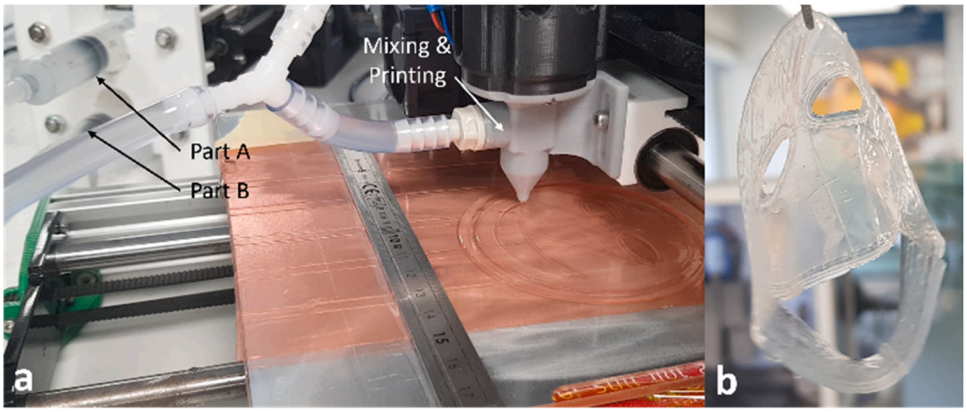

Fig. 7. Printed smiley-face without premixing. a) printing to realize the structure. b) final result of automatic 3D printing of two-part elastomer.

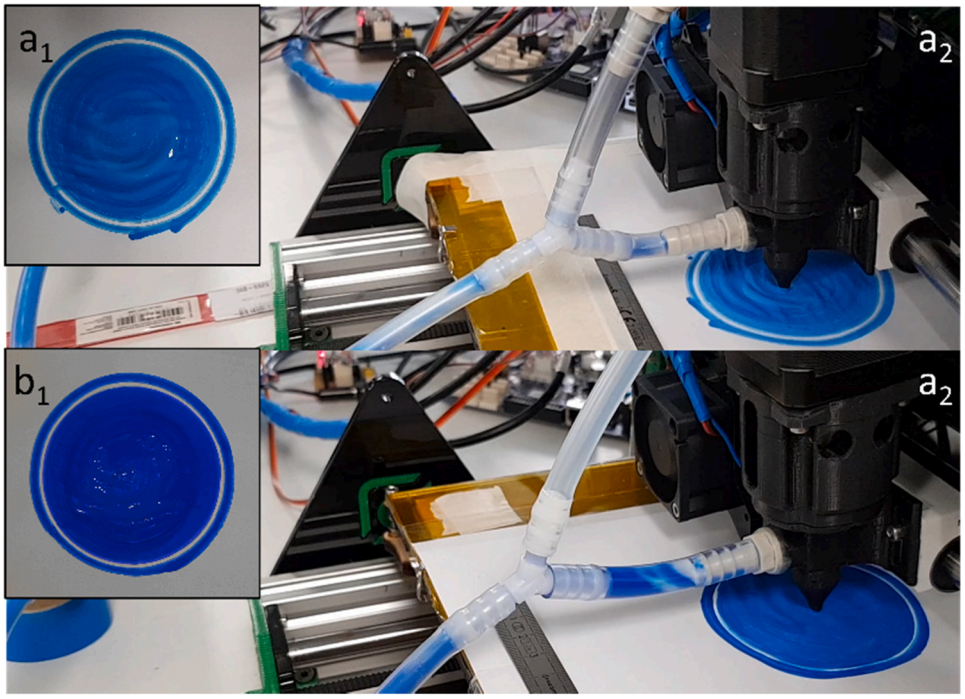

Fig. 8. Print of disk-like design on paper while two materials are mixed a_1) cylinder shape sample a_2) 3D printing of 1:1 ratio of dark blue and white colors b_1) cylinder shape sample b_2) 3D printing of 10:7 ratio of dark blue and white colors.

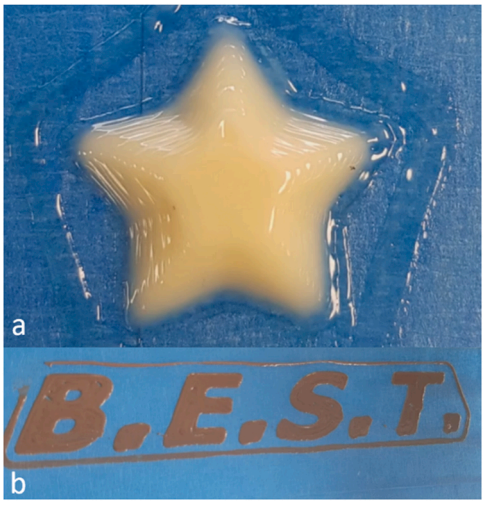

Fig. 9. Print of food related materials a) Star shape food additive b) 3D printing of 'BEST' with melted chocolate.

different types of materials. For example, the developed system was evaluated for its capability to print food-based materials such as mayonnaise (Hellmann's Real Mayonnaise) and melted chocolate (Galaxy Milk Chocolate) and the printed structures are shown in Fig. A syringe was filled with mayonnaise and placed on the PPS system without any other steps. The pressure was set to 1PSI and the printing speed was set at 5 mm/s. The total time for printing the structure was 10 min and the infill was 100 %. The chocolate on the other hand was firstly melted in an oven at 100 °C for 30 min to completely melt. Once the material was in a liquid form it was then mounted to the system. The pressure was set at 1.5 PSI and printing speed was 5 mm/s using the 1 mm diameter nozzle. Support Video 3 shows the printing of these structures. This approach could also be used for decoration of cakes or even for the automated preparation of food dishes.

4.4. Fully 3D printed embedded tactile sensor

In robotic applications, a major challenge is the fabrication of tactile sensors that are robust, soft, and low-cost. The system presented here, provides the ability to produce such tactile sensors in an automated process. To demonstrate this, we obtained the 3D printed tactile fingertip using the DIW system in combination with the FDM nozzle on the printer. The device has three embedded capacitive pressure sensors located at the tip, left, and right sides of the fingertip. All materials, including the encapsulation, conductive layer, and the dielectric (silicone), were 3D printed. The bottom part of the finger is made from PLA. The conductive plates of the sensors are fabricated using conductive PLA (Proto-pasta) filament using the FDM nozzle. Once the base and bottom electrodes were printed, the encapsulation layer made from Thermoplastic polyurethane (TPU) filament (NinjaFlex, NinjaTek) was printed using FDM nozzle. The device has three cavities which were filled with dielectric material using custom-made extruder system (Fig. 10a). After this, the material was left to cure for 3 h, while the heated bed was set to 40 °C. After this, a masking tape was placed on the surface of the dielectric layer, as printing directly on top of the dielectric was found to be challenging. Then, the printer continued printing the top electrodes and once those were printed, the material was changed to TPU to encapsulate the entire structure resulting in a soft 3D printed capacitive tactile finger with three embedded force sensors. Fig. 10b shows the finger pressed and the response of the sensor while Support Video 4 shows the entire process of realizing the device and the testing of the sensors. This approach of realizing tactile sensors provides a better control over the amount of materials used.

5. Conclusion

The current multimaterial 3D printers allow printing of one material at a time and offer limited opportunity for multiple materials mixing on the go. Despite several advances, the state-of-the-art FDM 3D printers offer limited cost-effective capability to fabricate multimaterial based complex smart structures. Other available 3D printers with similar capabilities are quite expensive. The new 3D printing extruder mechanism,

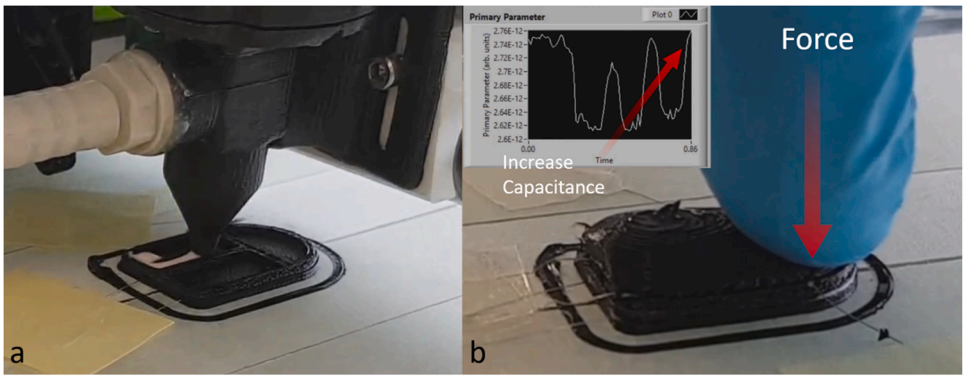

Fig. 10. 3D printed phalanx with embedded capacitive touch sensor. a) printing of the dielectric layer of the sensorised phalanx. b) testing of the sensorised phalanx for its response at different applied pressures.

presented in this work, shows the potential way for overcoming these challenges. The developed printer is able to print filaments and paste-like materials in the same print, while utilizing a pressure sensor for the feedback. The developed system utilizes the mounted syringes with different barrel diameters to mix multi-part materials (in desired ratios) needed to print complex 3D smart structures. As an example, the system can be used for fabrication of devices with composites that contain magnetic particles for actuation purposes. The results show that the presented extruder mechanism-based printer is able to handle diverse materials with different rheological properties. Furthermore, the system is free from common problems related to direct drive, Bowden tube, uncontrollable deposition as in pneumatic DIW systems, leaking, and delay between initiating printing and material deposition on the bed. The developed system does not rely on bulky equipment such as compressors, and thus offers better portability due to its reduced size and weight. The presented extruder mechanism is also capable of manufacturing complex structures in an automated manner and can be used for wide ranging applications that vary from food decoration to complex electronics and robotics.

CRediT authorship contribution statement

Ntagios Markellos: Writing – original draft, Validation, Software, Methodology, Investigation, Conceptualization. **Nassar Habib:** Writing – review & editing, Methodology. **Ravinder Dahiya:** Writing – review & editing, Writing – original draft, Visualization, Supervision, Resources, Project administration, Investigation, Funding acquisition, Formal analysis, Conceptualization.

Declaration of Competing Interest

The authors declare that they have no known competing financial interests or personal relationships that could have appeared to influence the work reported in this paper.

Data availability

Data will be made available on request.

Acknowledgements

This work was supported in part by the Engineering and Physical Sciences Research Council (EPSRC) through Engineering Fellowship for Growth – neuPRINTSKIN (EP/R029644/1), National Productivity Investment Fund (EP/R512266/1). The work presented in this paper was initiated by R. Dahiya's Bendable Electronics and Sensing Technologies (BEST) Group when he was at University of Glasgow, UK. The work got completed after he moved to Northeastern University, USA, where his group is known as Bendable Electronics and Sustainable Technologies (BEST) Group. Authors also acknowledge the support provided by Shadow Robot Company LTD, UK.

Appendix A. Supporting information

Supplementary data associated with this article can be found in the online version at doi:10.1016/j.addma.2023.103437.

References

[1] H. Bikas, P. Stavropoulos, G. Chryssolouris, Additive manufacturing methods and modelling approaches: a critical review, Int. J. Adv. Manuf. Technol. vol. 83 (1–4) (2016) 389–405.
[2] D.L. Bourell, Perspectives on additive manufacturing, Annu. Rev. Mater. Res. vol. 46 (2016).
[3] A. Vanderploeg, S.-E. Lee, M. Mamp, The application of 3D printing technology in the fashion industry, Int. J. Fash. Des. Technol. Educ. vol. 10 (2) (2017) 170–179.
[4] T.S. Srivatsan and T.S. Sudarshan, Additive manufacturing: innovations, advances, and applications 2015.
[5] A. Haleem, M. Javaid, Additive manufacturing applications in industry 4.0: a review, J. Ind. Integr. Manag. vol. 4 (04) (2019) 1930001.
[6] R. Dahiya, D. Sakthivel, and W.N. Taube, Three dimensional structure with sensor capability. Google Patents, May 27, 2021.
[7] M. Ntagios, R. Dahiya, 3D printed soft and flexible insole with intrinsic pressure sensing capability, IEEE Sens. J. (2022) 1, https://doi.org/10.1109/JSEN.2022.3179233.
[8] M. Ntagios, H. Nassar, A. Pullanchiyodan, W.T. Navaraj, R. Dahiya, Robotic hands with intrinsic tactile sensing via 3D printed soft pressure sensors, Adv. Intell. Syst. vol. 2 (6) (2020) 1900080, https://doi.org/10.1002/aisy.201900080.
[9] J.K. Placone, A.J. Engler, Recent advances in extrusion-based 3D printing for biomedical applications, Adv. Healthc. Mater. vol. 7 (8) (2018) 1701161.
[10] N. Shahrubudin, T.C. Lee, R. Ramlan, An overview on 3D printing technology: Technological, materials, and applications, Procedia Manuf. vol. 35 (2019) 1286–1296.
[11] D.-A. Türk, L. Triebe, M. Meboldt, Combining additive manufacturing with advanced composites for highly integrated robotic structures, Procedia CIRP vol. 50 (2016) 402–407.
[12] O. Ozioko, P. Karipoth, P. Escobedo, M. Ntagios, A. Pullanchiyodan, R. Dahiya, SensAct: the soft and squishy tactile sensor with integrated flexible actuator, Adv. Intell. Syst. vol. 3 (3) (2021) 1900145, https://doi.org/10.1002/aisy.201900145.
[13] R.L. Truby, et al., Soft somatosensitive actuators via embedded 3D printing, Adv. Mater. vol. 30 (15) (2018) 1706383, https://doi.org/10.1002/adma.201706383.
[14] M.R. Khosravani, T. Reinicke, 3D-printed sensors: Current progress and future challenges, Sens. Actuators A Phys. vol. 305 (2020), 111916.
[15] A. Christou, M. Ntagios, A. Hart, R. Dahiya, GlasVent—the rapidly deployable emergency ventilator, Glob. Chall. vol. 4 (12) (2020) 2000046.
[16] O. Ozioko, H. Nassar, R. Dahiya, 3D printed interdigitated capacitor based tilt sensor, IEEE Sens. J. vol. 21 (23) (2021) 26252–26260.
[17] J.J. Adams, et al., Conformal printing of electrically small antennas on three-dimensional surfaces, Adv. Mater. vol. 23 (11) (2011) 1335–1340.
[18] M. Areir, Y. Xu, D. Harrison, J. Fyson, 3D printing of highly flexible supercapacitor designed for wearable energy storage, Mater. Sci. Eng. B vol. 226 (2017) 29–38, https://doi.org/10.1016/j.mseb.2017.09.004.
[19] H. Nassar, A. Pullanchiyodan, M. Bhattacharjee, R. Dahiya, 3D printed interconnects on bendable substrates for 3D circuits, 2019 IEEE International Conference on Flexible and Printable Sensors and Systems (FLEPS) (2019) 1–3, https://doi.org/10.1109/FLEPS.2019.8792234.

[20] H. Nassar, R. Dahiya, Fused deposition modeling-based 3D-printed electrical interconnects and circuits, Adv. Intell. Syst. vol. 3 (12) (2021) 2100102, https://doi.org/10.1002/aisy.202100102.
[21] F. Liu, S. Deswal, A. Christou, Y. Sandamirskaya, M. Kaboli, R. Dahiya, Neuro-inspired electronic skin for robots, Sci. Robot. 7 (67) (2022), eabl7344, https://doi.org/10.1126/scirobotics.abl7344.
[22] F. Liu, et al., Printed synaptic transistor–based electronic skin for robots to feel and learn, Sci. Robot. 7 (67) (2022), eabl7286, https://doi.org/10.1126/scirobotics.abl7286.
[23] X. Wang, L. Dong, H. Zhang, R. Yu, C. Pan, Z.L. Wang, Recent progress in electronic skin, Adv. Sci. vol. 2 (10) (2015) 1500169, https://doi.org/10.1002/advs.201500169.
[24] M. Chakraborty, J. Kettle, R. Dahiya, Electronic waste reduction through devices and printed circuit boards designed for circularity, IEEE J. Flex. Electron. vol. 1 (1) (2022) 4–23.
[25] B.Y. Ahn, et al., Omnidirectional printing of flexible, stretchable, and spanning silver microelectrodes, Science (80-.) vol. 323 (5921) (2009) 1590–1593.
[26] H. Nassar, M. Ntagios, W.T. Navaraj, R. Dahiya, Multi-material 3D printed bendable smart sensing structures. 2018 IEEE SENSORS, 2018, pp. 1–4, https://doi.org/10.1109/ICSENS.2018.8589625.
[27] R. Chirila, M. Ntagios, R. Dahiya, 3D printed wearable exoskeleton human-machine interfacing device. 2020 IEEE SENSORS, 2020, pp. 1–4, https://doi.org/10.1109/SENSORS47125.2020.9278611.
[28] F. Wasserfall, D. Ahlers, N. Hendrich, and J. Zhang, 3D-printable electronics-integration of SMD placement and wiring into the slicing process for FDM fabrication, 2016.
[29] E.L. Gill, X. Li, M.A. Birch, Y.Y.S. Huang, Multi-length scale bioprinting towards simulating microenvironmental cues, Bio-Des. Manuf. vol. 1 (2) (2018) 77–88.
[30] S. Guo, F. Gosselin, N. Guerin, A. Lanouette, M. Heuzey, D. Therriault, Solvent-cast three-dimensional printing of multifunctional microsystems, Small vol. 9 (24) (2013) 4118–4122.
[31] M. Kahl, M. Gertig, P. Hoyer, O. Friedrich, D.F. Gilbert, Ultra-low-cost 3D bioprinting: modification and application of an off-the-shelf desktop 3D-printer for biofabrication, Front. Bioeng. Biotechnol. vol. 7 (2019) 184.
[32] S.V. Murphy, A. Atala, 3D bioprinting of tissues and organs, Nat. Biotechnol. vol. 32 (8) (2014) 773–785.
[33] D. Therriault, R.F. Shepherd, S.R. White, J.A. Lewis, Fugitive inks for direct-write assembly of three-dimensional microvascular networks, Adv. Mater. vol. 17 (4) (2005) 395–399.
[34] W. Martanto, S.M. Baisch, E.A. Costner, M.R. Prausnitz, M.K. Smith, Fluid dynamics in conically tapered microneedles, AIChE J. vol. 51 (6) (2005) 1599–1607.
[35] R. Karyappa, M. Hashimoto, Chocolate-based ink three-dimensional printing (Ci3DP), Sci. Rep. vol. 9 (1) (2019) 1–11.
[36] H. Zhang, S.K. Moon, Reviews on machine learning approaches for process optimization in noncontact direct ink writing, ACS Appl. Mater. Interfaces vol. 13 (45) (2021) 53323–53345.
[37] G. Wang, L. Yao, W. Wang, J. Ou, C.-Y. Cheng, H. Ishii, xPrint: a modularized liquid printer for smart materials deposition. Proceedings of the 2016 CHI conference on human factors in computing systems, 2016, pp. 5743–5752.
[38] C.G. Amza, A. Zapciu, D. Popescu, Paste extruder—hardware add-on for desktop 3D printers, Technologies vol. 5 (3) (2017) 50.
[39] M.A.S.R. Saadi, et al., Direct ink writing: a 3D printing technology for diverse materials, Adv. Mater. vol. 34 (28) (2022) 2108855, https://doi.org/10.1002/adma.202108855.
[40] M.A. Skylar-Scott, J. Mueller, C.W. Visser, J.A. Lewis, Voxelated soft matter via multimaterial multinozzle 3D printing, Nature vol. 575 (7782) (2019) 330–335, https://doi.org/10.1038/s41586-019-1736-8.
[41] D. Kokkinis, F. Bouville, A.R. Studart, 3D printing of materials with tunable failure via bioinspired mechanical gradients, Adv. Mater. vol. 30 (19) (2018) 1705808, https://doi.org/10.1002/adma.201705808.
[42] O. Rios, et al., 3D printing via ambient reactive extrusion, Mater. Today Commun. vol. 15 (2018) 333–336, https://doi.org/10.1016/j.mtcomm.2018.02.031.
[43] M.O.F. Emon, F. Alkadi, D.G. Philip, D.-H. Kim, K.-C. Lee, J.-W. Choi, Multi-material 3D printing of a soft pressure sensor, Addit. Manuf. vol. 28 (2019) 629–638, https://doi.org/10.1016/j.addma.2019.06.001.
[44] O. Uitz, P. Koirala, M. Tehrani, C.C. Seepersad, Fast, low-energy additive manufacturing of isotropic parts via reactive extrusion, Addit. Manuf. vol. 41 (2021), 101919.
[45] S. Romberg, C. Hershey, J. Lindahl, W. Carter, B.G. Compton, V. Kunc. Large-scale additive manufacturing of highly exothermic reactive polymer systems, Oak Ridge National Lab. (ORNL), Oak Ridge, TN (United States), 2019.
[46] V. Beedasy, P.J. Smith, Printed electronics as prepared by inkjet printing, Materials vol. 13 (3) (2020), https://doi.org/10.3390/ma13030704.
[47] A.A. Gupta, A. Bolduc, S.G. Cloutier, R. Izquierdo, Aerosol jet printing for printed electronics rapid prototyping. 2016 IEEE International Symposium on Circuits and Systems (ISCAS), 2016, pp. 866–869, https://doi.org/10.1109/ISCAS.2016.7527378.
[48] P. Jiang, Z. Ji, X. Zhang, Z. Liu, X. Wang, Recent advances in direct ink writing of electronic components and functional devices, Prog. Addit. Manuf. vol. 3 (1) (2018) 65–86.
[49] L. Nayak, S. Mohanty, S.K. Nayak, A. Ramadoss, A review on inkjet printing of nanoparticle inks for flexible electronics, J. Mater. Chem. C. vol. 7 (29) (2019) 8771–8795.
[50] M. Puertas-Bartolomé, M.K. Włodarczyk-Biegun, A. del Campo, B. Vázquez-Lasa, J. San Román, 3D printing of a reactive hydrogel bio-ink using a static mixing tool, Polymers vol. 12 (9) (2020), https://doi.org/10.3390/polym12091986.
[51] R. Dylla-Spears, et al., 3D printed gradient index glass optics, Sci. Adv. vol. 6 (47) (2023) eabc7429, https://doi.org/10.1126/sciadv.abc7429.
[52] V.G. Rocha, E. Saiz, I.S. Tirichenko, E. García-Tuñón, Direct ink writing advances in multi-material structures for a sustainable future, J. Mater. Chem. A vol. 8 (31) (2020) 15646–15657.
[53] K. Pusch, T.J. Hinton, A.W. Feinberg, Large volume syringe pump extruder for desktop 3D printers, HardwareX 3 (2018) 49–61.
[54] X. Wan, L. Luo, Y. Liu, J. Leng, Direct ink writing based 4D printing of materials and their applications, Adv. Sci. vol. 7 (16) (2020) 2001000.
[55] M. Schouten, G. Wolterink, A. Dijkshoorn, D. Kosmas, S. Stramigioli, G. Krijnen, A review of extrusion-based 3d printing for the fabrication of electro-and biomechanical sensors, IEEE Sens. J. vol. 21 (11) (2020) 12900–12912.